Protection and Control of Modern Power Systems

ORIGINAL RESEARCH Open Access

Annual performance analysis of different maximum power point tracking techniques used in photovoltaic systems

Y. Chaibi[1*], A. Allouhi[2], M. Salhi[1] and A. El-jouni[3]

Abstract

This paper presents an annual performance evaluation of three maximum power point tracking (MPPT) methods. The used MPPT techniques (Perturb and Observe, Incremental Inductance and Sliding mode) are evaluated under an annual data of atmospheric conditions of the target site. The main contribution of this work is to consider real fluctuation conditions of solar irradiations, ambient temperatures and wind velocities. It was found that the Sliding mode provides higher energy yields independently of the period. Compared to the basic P&O and the IC techniques, sliding mode has the potential of generating up to 8.18% more electrical energy than other techniques.

Keywords: Photovoltaic systems, Maximum power point tracking (MPPT), Annual performance

1 Introduction

In the last decades, according to statistic [1], the world energy need exhibits a rapid growth, which caused a huge production of electricity with different polluting sources as natural gas, oil and coal [2]. Nowadays, the excessive use of these fossil sources has a negative effect from both economic and environment point of views. In fact, the economic consequence is presented by the high increase of petroleum's price which leads directly to a rise of the electricity tariff. For the environmental impact, the emission of CO_2 accentuating the damaging effects of climate change remains the major issue [3, 4]. In order to overcome these complications, leader countries in energy production have imposed a new policy that encourages the use of renewable energies due to its clean behavior and limitless quantity [5].

Today, diverse renewable energy sources are developed, such as solar, wind, hydro and geothermal. Due to their huge potential, these sources of energy are being used increasingly in industrial and buildings sectors. Solar energy at the top of renewable energy sources is believed to cover a significant part of energy needs in several countries. More specifically, photovoltaic systems due to their simple implementation and low maintenance cost, can provide clean and sustainable electricity. Power generated from photovoltaic modules can be used in grid-connected and stand-alone systems [6, 7]. Grid-connected PV systems are developed to operate with the electric utility grid and offer the possibility of covering energy requirements of the structure with capability of selling the rest of produced energy to electricity supplier [8]. Stand-alone PV systems, in turn, are used to supply electricity needed in isolated sites and as well for agricultural pumping [9, 10].

The weakness of PV systems lies in the low conversion efficiency because of the nonlinearity behavior of the PV cell. This requires the use of maximum power point tracking (MPPT) controllers with the aim of forcing the PV panel to operate at its maximum power point (MPP) despite the changes in outdoor climatic conditions [11, 12]. Mathematically, to ensure the function of maximizing the PV power, a derivative of the PV power P_{pv} with respect to the PV voltage V_{pv} must converge to zero [13, 14]. For this reason, several algorithms have been developed and improved [15–18]. The most popular one is the classical perturb and observe (P&O) method [19, 20]; this technique is based on perturbing the PV voltage and observing the MPP variation, the history of this method is known by its several improved versions. Starting with the variable step P&O, where the perturbation is adapted to the operating

* Correspondence: chaibi.yassine@gmail.com; y.chaibi@edu.umi.ac.ma
[1]2EMI team, ENSAM, Moulay Ismail University, 50500, B.P 15290 El Mansour, Meknes, Morocco
Full list of author information is available at the end of the article

point area. As reported in [21], Kullimalla et al. adjusted the step size to raise the tracking speed and to reduce the oscillating, this adaptive method shown an operating point closer to the MPP and presented a fast response compared to conventional algorithms, furthermore, other researchers such as Hong et al. has developed an adaptive step size according to the error [22], this solution presented a high tracking performance with low power losses compared to other P&O algorithms. Although, these improved versions of the P&O have arrived to ameliorate the tracking performance but the oscillating around MPP stills the principal cause of energy losses, especially in fast irradiance change. To overcome this issue, other techniques such as the incremental conductance (IC) are required [23, 24]. The IC tracks the MPP by comparing instantly the conductance with the incremental conductance of the PV module [25]. To perform at the MPP, both quantities must be equal. For this reason, the IC method presented the conventional version with a fixed step adapted to the operating zone [26]. Unfortunately, the fixed step IC shown a low response under fast irradiance change. Then, Incremental Conductance with variable step corrected partially this problem and becomes widely used. Lui et al. [27], Emad et al. [28] used the variable step, where the slope of the P-V characteristic is multiplied with the fixed step, which enhanced the tracking speed and shown a superiority compared to the conventional fixed step algorithms. As a result, most of improved version of this technique corrected partially the problem of oscillation and shown a remarkable performance under fast change of atmospheric conditions.

In order to improve the sensitivity of the PV module at the optimal point, artificial intelligence as fuzzy logic [29, 30]; and neuron network algorithms are used [31, 32]. However, the complexity of these methods makes them hard to implement in real life since they need high-performance calculator to ensure the maximum power tracking operation. Accordingly, to have a good compromise between efficiency and cost, numerical theories such as Backstepping and Sliding mode are employed to build an improved MPPT that satisfy the conditions of both good performance and low-cost [33].

The sliding mode MPPT (SM-MPPT) is a nonlinear control technique based on the design of a control law that forces the system trajectory to reach the sliding surface. Thanks to its advantages such as a robust behavior in the presence of external variation and the simplicity of implementation. In literature, various controllers have been proposed [34–36]. Dahech et al. proposed a robust controller using both the Backstepping and the sliding mode and this hybrid method offered a MPPT controller with high efficiency and low error of tracking [37]. Moreover, an adaptive SM-MPPT has been proposed by Koofigar et al. with the aim objective to overcome all the problem caused by external uncertainties, this improved method shown a very high performance of tracking even with fast climate variations [38]. Hence, most of MPPT based on sliding mode show a very high performance and stability with fast atmospheric changes.

In this paper, the effect of MPPT algorithm on the net energy output of solar PV modules is investigated. For this end, three different MPPT algorithms are tested on the PV system in Fig. 1. The innovative aspect met in this paper is the utilization of real climatic conditions evaluated for duration of one complete year (8760 running hours). A strong calculation effort has been made, as it was essential to fit hourly data to comply well with the time step used in the simulation process. To the best of knowledge of authors, although there are many published papers comparing various MMPT control techniques, a realistic approach to quantify the differences induced in the associated energy yields is missed. The conclusions outlined in this paper can offer guidelines about the development and cost-effectiveness of MPPT techniques in their design phase.

2 Methods

2.1 PV system modeling

2.1.1 PV module

PV module is a group of cells connected in series or in parallel with the main objective to convert sunlight into electricity via the photodiode operation, the latter is explained by the p-n junction phenomenon and the produced current depends on the received irradiance and temperature [39]. The PV cell is represented electrically by several equivalent circuit models [40, 41]. Fig. 2 shows one of the most used models, which is called the one diode model and composed of a diode in parallel with a courant source, shunt and series resistances [39].

By using Kirchhoff's law, the output generated current by the PV module is given by:

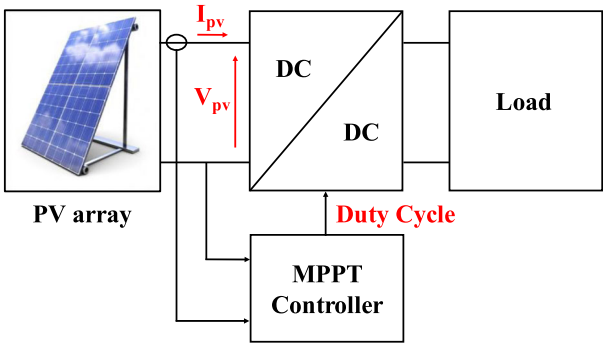

Fig. 1 The used configuration of the PV system

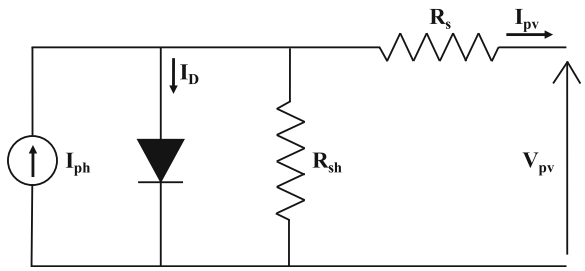

Fig. 2 Single diode equivalent model of the PV cell

$$I_{pv} = I_{ph} - I_{os}\left\{\exp\left[A\left(V_{pv} + I_{pv}R_s\right) - 1\right]\right\} - \frac{V_{pv} + R_s I_{pv}}{R_{sh}} \tag{1}$$

with

$$A = \frac{q}{\gamma k T_{cell} N_{cell}}$$

I_{ph} is the light-generated current with the value depends on irradiance and temperature levels, and this current is expressed by the following equation:

$$I_{ph} = \left[I_{sc} + K_i\left(T_{cell} - T_{ref}\right)\frac{\lambda}{\lambda_{ref}}\right] \tag{2}$$

From the Shockley equation, the cell reverse current I_{os} can be presented by the Eq. (3), this current depends only on the temperature variation:

$$I_{os} = I_{or}\left(\frac{T_{cell}}{T_{ref}}\right)^3 \exp\left(\frac{qE_G}{k\gamma}\left[\frac{1}{T_{cell}} - \frac{1}{T_{ref}}\right]\right) \tag{3}$$

In order to adjust the supply power to the used one, several PV panels are connected in series and in parallel to form a PV array and the total current is given by:

$$I_{pvg} = N_p I_{ph} - N_p I_{os}\left\{\exp\left[\frac{A}{N_s}\left(V_{pv} + I_{pv}R_s\frac{N_s}{N_p}\right) - 1\right]\right\} - \frac{V_{pv} + I_{pv}R_s\frac{N_s}{N_p}}{R_{sh}\frac{N_s}{N_p}} \tag{4}$$

2.1.2 DC-DC converter

DC-DC boost converter is an adaptation stage mostly used after the PV array in order to adjust the supplied voltage to the load, another function of this converter is allowing the PV system to perform at its MPP by acting on the cyclic duty D, this task is executed by the boost capability of delivering an output voltage V_{DC} larger than the input one V_{pv} [42]. This voltage is defined as:

$$V_{DC} = \frac{V_{pv}}{1\text{-}D} \tag{5}$$

Fig. 3 shows the used configuration of the boost converter. The system in state average values can be written as:

$$\begin{cases} \dfrac{\partial v_{pv}}{\partial t} = \dfrac{1}{C}\left(i_{pv} - i_L\right) \\ \dfrac{\partial i_L}{\partial t} = \dfrac{1}{L}\left[v_{pv} - (1-D)v_{DC}\right] \\ \dfrac{\partial v_{DC}}{\partial t} = \dfrac{1}{C_{DC}}\left[i_L(1-D) - i_o\right] \end{cases} \tag{6}$$

where, v_{pv}, v_{DC}, i_L and i_O and are respectively the PV voltage, the boost output voltage, the inductor current and the boost output current, C and L represent the input capacitor and inductor of the converter and C_{DC} is the output capacitor.

2.2 Examined MPPT techniques

2.2.1 Perturb and observe algorithm

The P&O algorithm is an iterative technique performed by perturbing the measured voltage V_{pv} with ΔV until reaching the PV power P_{pv} to its MPP. The P-V characteristic is divided into three operating regions as follows [20]:

- If $\frac{\partial P_{pv}}{\partial V_{pv}} > 0$: operating point is on the left of the MPP.
- If $\frac{\partial P_{pv}}{\partial V_{pv}} < 0$: operating point is on the right of the MPP.
- If $\frac{\partial P_{pv}}{\partial V_{pv}} = 0$: operating point is at the MPP.

The flowchart of the P&O algorithm is presented in Fig. 4. As can be seen, the process of extracting still working even after reaching the MPP which causes oscillation around this point infinitely [19].

2.2.2 Incremental conductance algorithm

The incremental conductance technique is developed to correct partially the oscillation problem caused by different iterative techniques. The idea behinds the IC method is to compare the PV conductance $(\frac{I_{pv}}{V_{pv}})$ with the derivative conductance $(\frac{\Delta I_{pv}}{\Delta V_{pv}})$ instantly [43]. The operating zones are given as follows [23]:

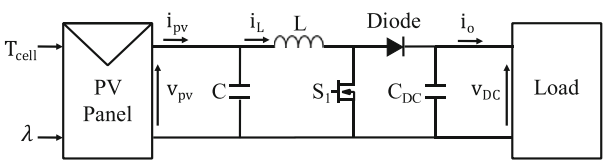

Fig. 3 The schematic of the DC-DC boost converter

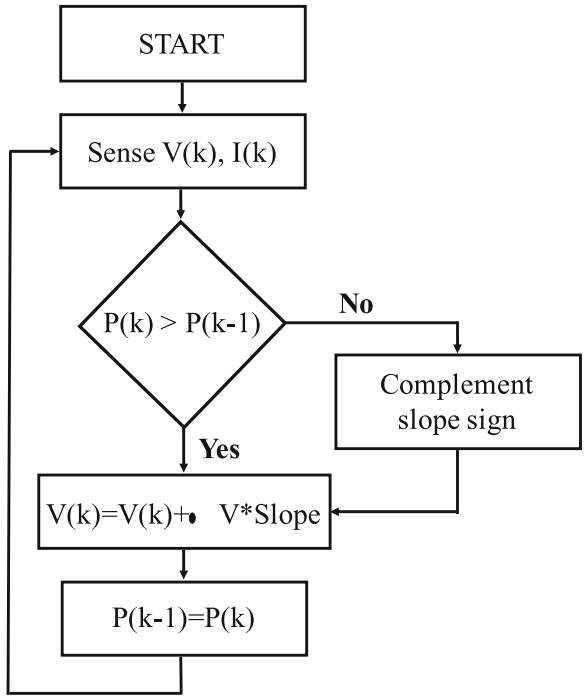

Fig. 4 The flowchart of the P&O-MPPT method

- If $\frac{\Delta I_{pv}}{\Delta V_{pv}} > -\frac{I_{pv}}{V_{pv}}$: operating point is on the left of the MPP.

- If $\frac{\Delta I_{pv}}{\Delta V_{pv}} < -\frac{I_{pv}}{V_{pv}}$: operating point is on the right of the MPP.

- If $\frac{\Delta I_{pv}}{\Delta V_{pv}} = -\frac{I_{pv}}{V_{pv}}$: the operating point is at the MPP.

Fig. 5 gives the flowchart of the incremental conductance which respects previous conditions. As

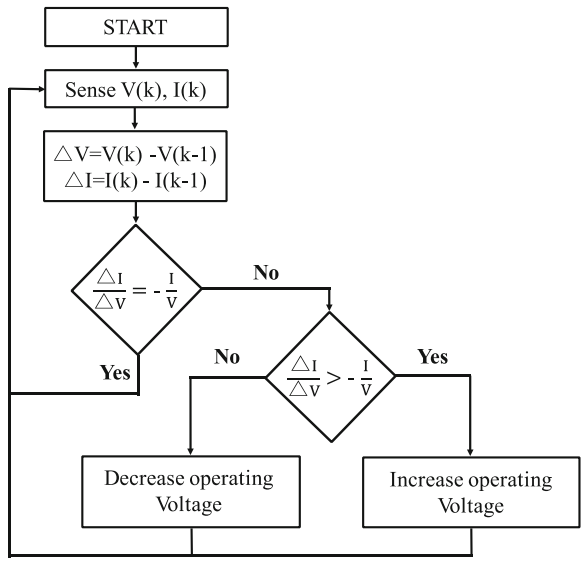

Fig. 5 The flowchart of the IC-MPPT method

reported in a precedent work [26–28], the main advantage of this technique is the good performance under fast-changing climate conditions and a lower oscillation around the MPP comparing to the P&O technique. However, the weakness of this method is the inability to achieve the zero-point condition which causes some power losses [26].

2.2.3 Sliding mode MPPT

The sliding mode theory allows to design MPPT controller with a robust behavior in presence of external disturbances such as temperature and irradiance variations. This method consists in varying the state trajectory of the system to a predefined sliding surface [23, 36, 44]. This function is achieved by developing a control law which forces the output $y = \frac{\partial P_{pv}}{\partial V_{pv}}$ to converge to zero [36].

The methodology of the sliding mode is presented as follows:

First, choosing a sliding surface, also called the switching surface which depends on the relative degree r of the system and the output y. For the used PV system in Fig. 3, this surface can be expressed by Eq. (7):

$$\sigma = \dot{y} + \beta y \tag{7}$$

and

$$\dot{\sigma} = \ddot{y} + \beta \dot{y} \tag{8}$$

where $\dot{y}$ and $\ddot{y}$ are respectively the first and the second time derivative of the output y and β is a positive constant. The time derivative of the sliding surface can be written as:

$$\dot{\sigma} = f + gu \tag{9}$$

with

$$u = \frac{1}{1-D}$$

Then, designing of the control law in order to ensure the stability of the system, the Lyapunov function defined by $V = \frac{1}{2}\sigma$ is adopted, only the $\dot{V} < 0$ allows the stability.

By choosing the dynamic function as: $\dot{\sigma} = -m\ \text{sign}(\dot{\sigma})$.

$$\dot{V} = -m|\sigma| \tag{10}$$

From precedent equations, the control law is given by:

$$\begin{cases} u = -\frac{f + m.\ \text{sign}(\sigma)}{g} \\ D = 1 + \frac{g}{f + m.\ \text{sign}(\sigma)} \end{cases} \text{ with } m > 0.$$

3 Results and discussion

The performance of any PV system depends on its behavior under atmospheric variations such as the change

of irradiance, temperature and wind velocity. For this reason, a PV array composed of 100 PV modules with the technical specifications listed in Table 1 has been simulated under real climatic data of Fez, Morocco.

Hourly meteorological data were exported from METENORM software. The first set of results pertains power outputs of PV array on a daily basis. Later, an overall comparison in terms of net energy output generated from PV modules operating with the MPPT techniques is presented.

3.1 Daily analysis

In Fig. 6a,b,c d, climatic variations of the first day of each season are presented. Because the PV system is tested under the change of the irradiance and cell temperature, the cell temperature calculations are based on the model given by Duffie et al. in Eq. (A.1) [45].

Table 2 gives the maximum values of the used climate conditions for each day. As shown from this table, for September 21, the maximum incident irradiance is about 1043.4 W/m^2. For the other atmospheric conditions, June 21 recorded the maximum values of the ambient temperature, cell temperature and the wind speed. The corresponding values are respectively, 36 °C for ambient temperature, 62.27 °C for cell temperature and 9.8 m/s for the wind speed. In addition, the coldest scenario, presented by December 21 shows minimum values of ambient and cell temperatures as well as incident solar radiations.

In order to evaluate the proposed MPPT controllers, the generated power from the Monocrystalline SM55 PV array is provided in Fig. 7a,b,c,d. This output corresponds to the climatic data previously presented. As can be observed, the SM-MPPT presents a remarkable superiority in terms of level of power tracking and this is true independently of the examined day. However, the P&O MPPT and the IC-MPPT exhibit approximately the same profiles for all the seasons except for the first

Table 1 Evaluation data and result (portion)

Parameters	Mono-Si SM55	Poly-Si MSX60
P_m [W]	55	60
V_m [V]	17.4	17.1
I_m [A]	3.15	3.5
V_{oc} [V]	21.7	21.1
I_{sc} [A]	3.45	3.8
K_i [%/K]	0.04	0.06
K_v [%/K]	−0.35	−0.37
N_{cell}	36	36
N_s	20	20
N_p	5	5
A_m [m^2]	0.42	0.55

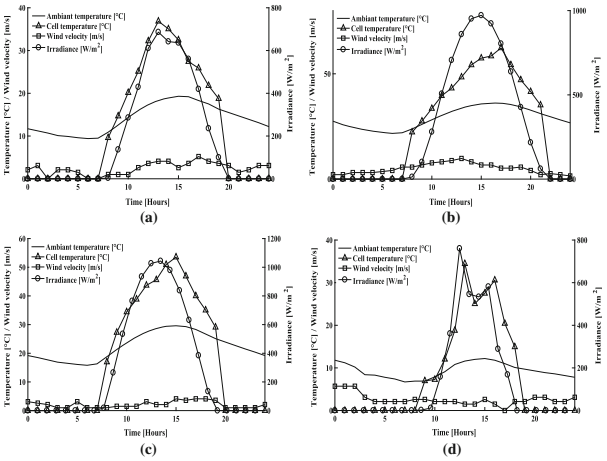

Fig. 6 Different daily atmospheric conditions for **a** March 21, **b** June 21, **c** September 21, **d** December 21

day of the winter because of the rapid fluctuations of cell temperature and irradiance. As seen in the Fig. 7d, the P&O technique shows high tracking performance compared the IC one.

Another performance index to be assessed is the real electric efficiency which can be computed using Eq. (A.2) formulated in the appendix.

According to SAM software [46], the nominal module efficiency of the Mono-Si SM55 is about 12.89%. In Fig. 8a,b,c,d, it is noticed that the SM-MPPT reaches rapidly the steady-state of the efficiency and remains around the nominal value. For the P&O and the IC MPPT, the efficiencies are similar except for the winter day because of the fast changes of temperature and irradiance. Also, the P&O shows slightly better efficiency compared to IC method.

With the same methodology used in the previous paragraphs, the Poly-Si MSX60 PV array with the technical specifications shown in Table 1 is simulated under the same conditions displayed in Fig. 6a,b,c,d. Fig. 9a,b,c,d presents the daily generated power using the examined MPPT techniques. As can be seen in this illustration, the generated power using the SM-MPPT confirms the high tracking performance and stability of this technique even with the Poly-Si technology. In fact, the SM-MPPT is known as a robust controller even with an external disturbance. On the other hand, and especially for the

Table 2 Maximum values of atmospheric condition for the used days

	March 21	June 21	September 21	December 21
λ_{max}[W/m^2]	686.03	971.96	1043.40	760.53
$T_{a\ max}$ [°C]	19.20	36	29.6	12.2
$T_{C\ max}$ [°C]	36.85	62.27	53.52	34.45
$v_{w\ max}$ [m/s]	5.2	9.8	4.1	5.7

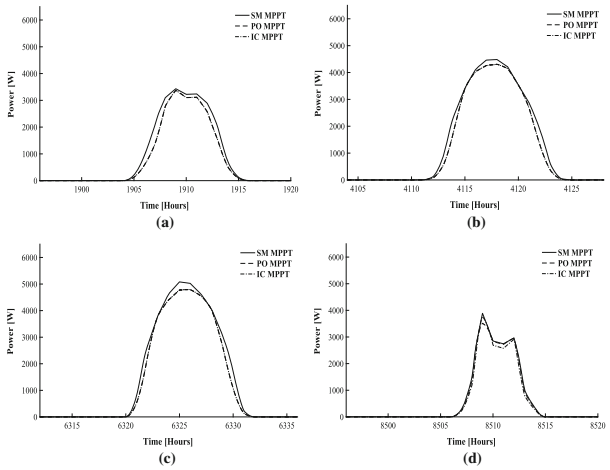

Fig. 7 Daily generated power using different MPPT techniques on the Mono-Si PV array SM55 for **a** March 21, **b** June 21, **c** September 21, **d** December 21

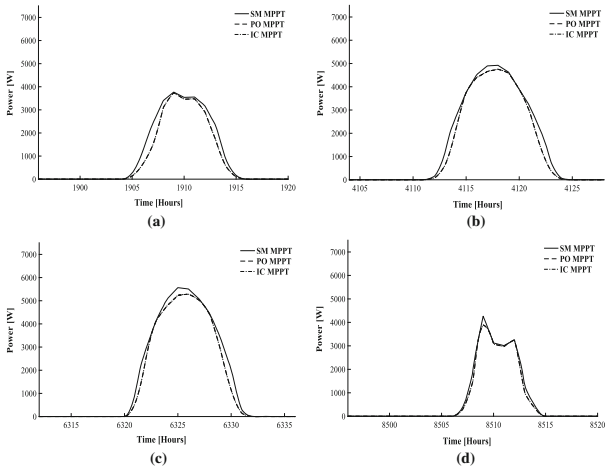

Fig. 9 Daily generated power using different MPPT techniques on the Poly-Si PV array MSX60 for **a** March 21, **b** June 21, **c** September 21, **d** December 21

Poly-Si technology, the P&O and the IC methods fit perfectly because of its similar approach followed to pursuit the MPP.

The module efficiency of the MSX 60 is plotted in Fig. 10a,b,c,d. According to SAM software [46], the nominal module efficiency of the MSX60 is given by a value of 10.80%. As can be seen in Fig. 10a,b,c,d, both the P&O and the IC method are identical in all cases of atmospheric variations, but the drawbacks of these methods is the low response to attain the steady-state around the nominal efficiency, which causes a lot of losses comparing to the sliding mode technique.

From this analysis, it was concluded that the sliding mode MPPT presents a very good solution to track the MPP comparing to the P&O and the IC methods. This superiority is proved from the reached efficiency and the good stability achieved by the SM-MPPT. Furthermore, this MPPT technique has a high tracking speed capability which allows transferring the PV energy with minimum losses.

3.2 Annual analysis

Because the daily analysis evaluates the performance of the PV system in a limited period, it is essential to quantify the net energy output of PV arrays generated in single Typical Meteorological Year. Similarly, meteorological data of Fez are used in the calculations. This location is known with high potential of solar energy and a hot weather in the summer and a cold one in the winter. Figs. 11, 12, 13 and 14 give respectively the annual values of ambient temperature, cell temperature, global incident irradiance and wind velocity. The

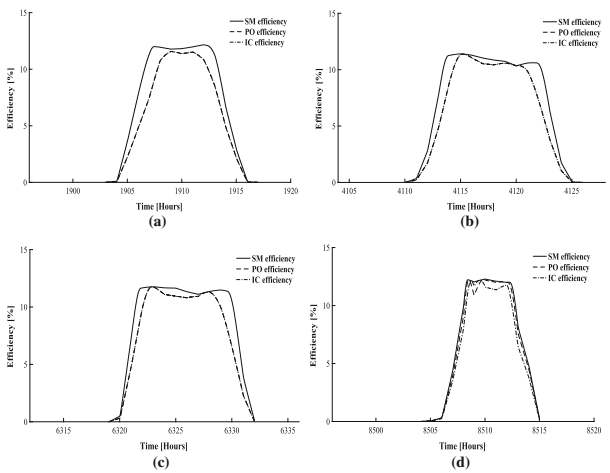

Fig. 8 Module Efficiencies using different MPPT techniques on the Mono-Si PV array SM55 for **a** March 21, **b** June 21, **c** September 21, **d** December 21

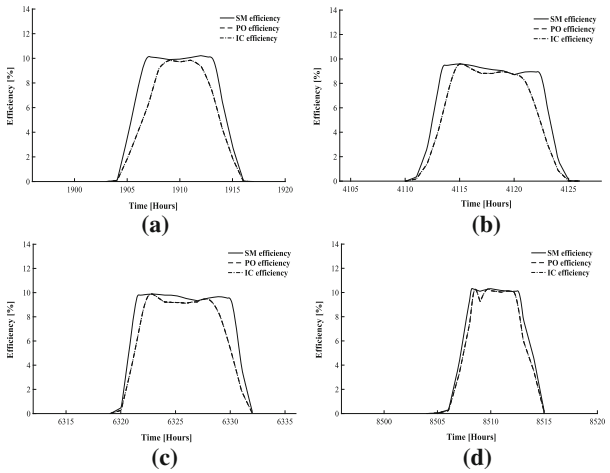

Fig. 10 Module Efficiencies using different MPPT techniques on the Poly-Si PV array MSX60 for **a** March 21, **b** June 21, **c** September 21, **d** December 21

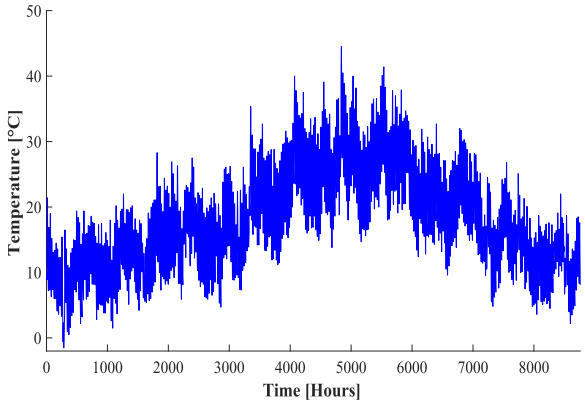

Fig. 11 Annual database of the ambient temperature [°C]

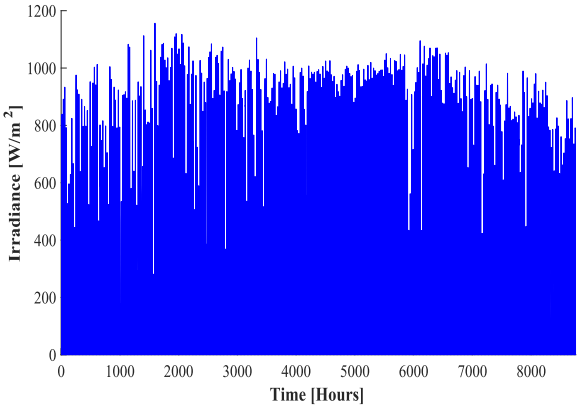

Fig. 13 Annual database of the irradiance [W/m^2]

presented data were generated on an hourly basis and fitted using the MATLAB toolbox to comply with the time step of 1 s used in the simulation processes.

As observed in Fig. 11, the annual ambient temperature varies between a maximum value of 44.5 °C and a minimal one of − 1.5 °C, this database is characterized by the different profiles of daily weathers (sunny, cloudy and mixed days). Fig. 12 gives the annual cell temperature using the NOCT model [47]; the daily peak of this temperature varies between 17.26 °C and 71.96 °C. Fig. 13 shows the annual irradiance in the same region. The daily peak irradiance changes between a value of 281.1 W/m^2 and 1156 W/m^2. In Fig. 14, the annual wind velocity is presented; the wind speed interval varies between 0 m/s and 16.5 m/s.

The simulation of the selected MPPT controllers (Sliding mode MPPT, P&O and IC) using the previous data. The annual generated power using the different MPPT techniques considering the two module technologies (Mono-Si SM55 and Poly-Si MSX60) are presented respectively in Fig. 15a,b,c and Fig. 16a,b,c.

By using the output results of the annual generated power, the annual produced energy is calculated using Eq. (A.3) in the Appendix.In Fig. 17, the calculated power is plotted for each technology using the selected MPPT technique; as shown in this figure, the annual produced energy using the SM-MPPT shows a considerable superiority for both technologies comparing to other MPPT techniques, to prove that, the relative gain given by Eq. (A.4) is calculated. These relative gains are presented in Table 3.

As can be observed, the sliding mode MPPT offers more energy outputs than the other techniques. For the Mono-Si technology, the relative gains generated by using the SM-MPPT compared to of the P&O and IC techniques. More specifically, in terms of yearly energy output, SM-MPPT could achieve up to 8.18% higher energy productions if PO and the IC methods. Moreover, the technology of PV modules seems to have a significant impact on the net relative energy gain induced. Higher rates are observed for the Poly-Si modules. At this point, it is interesting to note that further

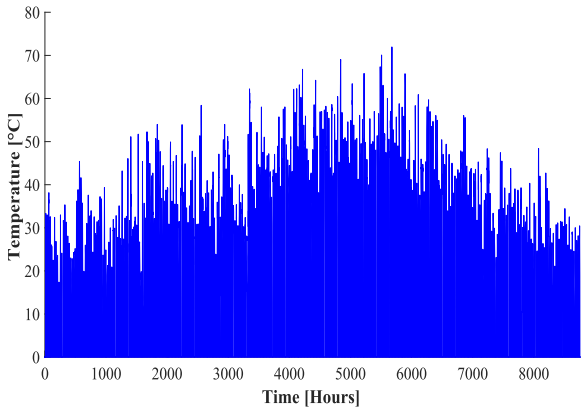

Fig. 12 Annual database of the cell temperature [°C]

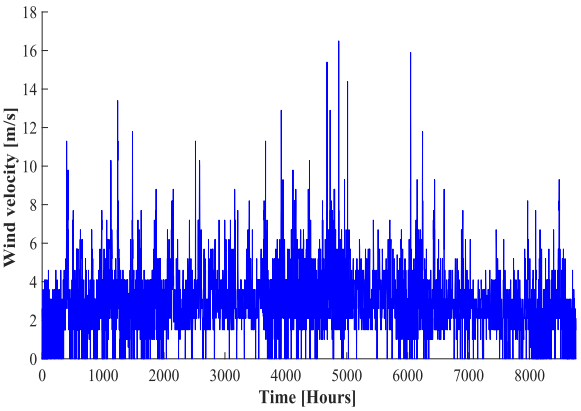

Fig. 14 Annual database of the wind velocity [m/s]

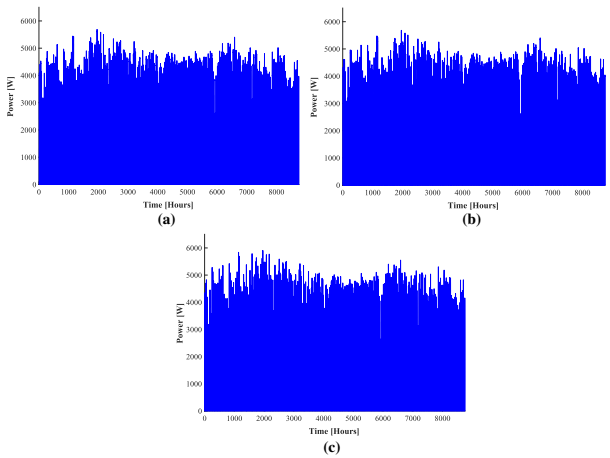

Fig. 15 Annual generated power using different MPPT techniques on SM55 PV array **a** P&O MPPT, **b** IC MPPT, **c** SM-MPPT

investigations should be undertaken to compare such techniques for other climate conditions and for other PV technologies to gather more information about the choice of a MPPT control technique.

4 Conclusion

This paper examines to what extent the MPPT technique could affect the yearly energy output of a solar photovoltaic field. To draw useful conclusions about this effect, running simulations based on real meteorological and operating conditions is essential. Considering one Typical Meteorological Year for the Moroccan city (Fez), a comparison between three MPPT techniques has been made in terms of daily, annual energy outputs and conversion efficiencies of a solar field comprising 100 PV modules. Poly-crystalline and Mono-crystalline silicon

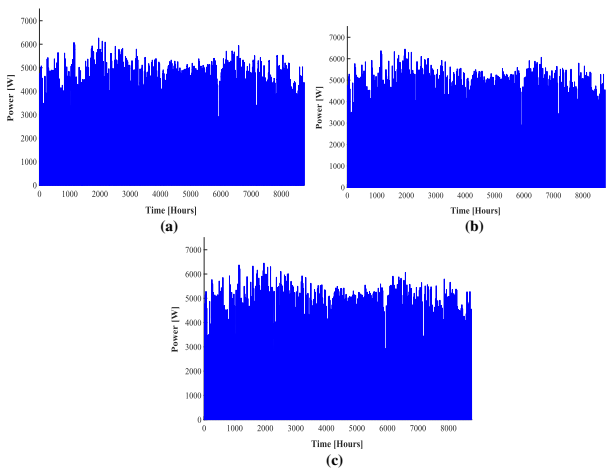

Fig. 16 Annual generated power using different MPPT techniques on the Poly-Si MSX60 PV array **a** P&O MPPT, **b** IC MPPT, **c** SM-MPPT

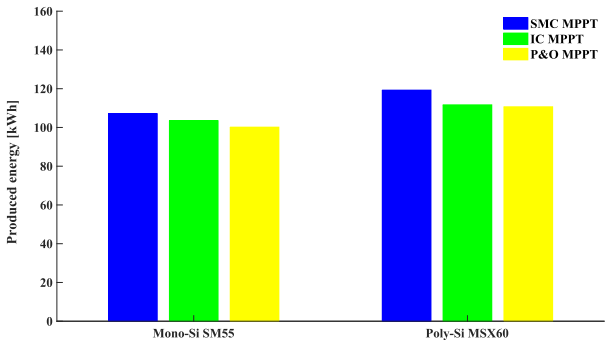

Fig. 17 Annual produced PV energy using different MPPT techniques for the Mono-Si SM55 and the Poly-Si MSX60 PV arrays

PV technologies have been tested. The total installed capacity is 6 kWp and 5.5 kWp, respectively. The main findings of this work can be summarized as follows:

- SM-MPPT yields the highest energy outputs annually compared to the P&O and IC techniques.
- In terms of yearly energy output, SM-MPPT could achieve up to 8.18% higher energy productions if compared to PO and the IC methods.
- Technology of PV modules has a significant impact on the net relative energy gain induced. Higher rates are observed for the Poly-Si modules.

Further investigations should be undertaken to compare such techniques for other climate conditions and for other PV technologies to gather more information about the appropriate choice of a MPPT control technique.

4.0.0.1 Nomenclatures

A_m module surface [m^2]
D duty cycle of the DC-DC converter
E_{GO} band gap for silicon [=1.22 eV]
I_{pv} output current of the PV panel [A]
I_m maximal current at MPP [A]
I_{or} saturation current of the PV panel [A]
I_{os} reverse saturation current of the PV panel [A]
I_{sc} short-circuit current [A]
I_{sol} light photo-current [A]
k Boltzmann's constant
K_i temperature coefficient of I_{sc} [A/K]
N_{cell} number of cells in series

Table 3 Relative energy gains in terms of the annual produced energy. Base case: SM-MPPT

	Mono-Si SM55	Poly-Si MSX60
ERG% [P&O]	7	8.18
ERG% [IC]	3.88	7.20

N_s number of modules in series
N_p number of modules in parallel
P_m maximum power at optimal operating point [W]
q electron charge
R_s series resistance [Ω]
R_{sh} shunt resistance [Ω]
T_c cell temperature [K]
T_{ref} reference temperature [= 298.15 K]
V_{pv} output voltage of the PV panel [V]
V_m maximum power voltage at MPP [V]
V_{oc} open circuit voltage [V]
γ ideality factor
λ solar irradiation [W/m^2]
λ_{ref} reference solar irradiance [=1000 W/m^2]

5 Appendix

The NOCT model temperature is given by the following equation:

$$T_c = T_a + \frac{\lambda}{800}(T_{NOCT}-20) \times \left(1-\frac{\eta_{ref}}{\alpha\tau}\right)\frac{9.5}{5.7+3.8v_w} \quad (A.1)$$

where, T_a is the ambient temperature, T_{NOCT} is the nominal operating cell temperature defined at ($\lambda = 800$ W/m^2, $T_a = 20\,^\circ$C, $v_w = 1$ m/s), η_{ref} is the reference module efficiency, $\alpha\tau$ is the transmittance-absorbance product and v_w is the wind velocity.

The module efficiency is given by:

$$\eta = \frac{P_{pv}}{A_m\lambda} \quad (A.2)$$

The annual produced energy is calculated using the following equation:

$$E_{pv} = \frac{1}{3600}\int_0^T P_{pv}dt \quad (A.3)$$

Where T is the final second of the year and the step of integration is chosen as 1 s.

The gain relative error is presented as follows:

$$ERG\% = \frac{E_R-E_C}{E_C}*100 \quad (A.4)$$

where E_R is the reference energy chosen as the produced energy using the SM-MPPT, E_C is the compared energy.

Acknowledgements
Not applicable.

Authors' contributions
YC and AA proposed the idea and the structure of the paper. YC modeled the proposed. PV system under MATLAB. YC and AA wrote the paper. AA, MS and AELJ contributed to reviewing the paper. All authors of this research paper have directly participated in the planning, execution, or analysis of this study. All authors read and approved the final manuscript.

Funding
The authors declare that they have no funding for the research.

Availability of data and materials
The data used to support the findings of this study have not been made available because it is confidential.

Competing interests
The authors declare that they have no competing interests.

Author details
[1]2EMI team, ENSAM, Moulay Ismail University, 50500, B.P 15290 El Mansour, Meknes, Morocco. [2]Ecole Supérieure de Technologie de Fès, U.S.M.B.A, Route d'Imouzzer, BP 2427, Fez, Morocco. [3]Physics Department of the CRMEF, Tangier, Morocco.

Received: 13 April 2019 Accepted: 30 July 2019
Published online: 28 August 2019

References

1. BP. (2017). BP Statistical Review of World Energy 2017. *British Petroleum*, 1–52.
2. Kousksou, T., Allouhi, A., Belattar, M., Jamil, A., El Rhafiki, T., Arid, A., et al. (2015). Renewable energy potential and national policy directions for sustainable development in Morocco. *Renewable and Sustainable Energy Reviews, 47*, 46–57.
3. da Silva, J. A. M., & de Oliveira Junior, S. (2018). Unit exergy cost and CO2emissions of offshore petroleum production. *Energy, 147*, 757–766.
4. Kahouli, B. (2018). The causality link between energy electricity consumption, CO2 emissions, R&D stocks and economic growth in Mediterranean countries (MCs). *Energy, 145*, 388–399.
5. Ellabban, O., Abu-Rub, H., & Blaabjerg, F. (2014). Renewable energy resources: Current status, future prospects and their enabling technology. *Renewable and Sustainable Energy Reviews, 39*, 748–764.
6. Lee, K. J., Shin, D. S., Lee, J. P., Yoo, D. W., Choi, H. K., & Kim, H. J. (2012). Hybrid photovoltaic/diesel green ship operating in standalone and grid-connected mode in South Korea - Experimental investigation. In *2012 IEEE Veh Power Propuls Conf VPPC* (Vol. 49, pp. 580–583).
7. Zheng, Z., Zhang, T., & Xue, J. (2018). Application of fuzzy control in a photovoltaic grid-connected inverter. *Journal of Electrical Computer Engineering, 2018*, 1–10.
8. Del Fabbro, B., Valentinčič, A., & Gubina, A. F. (2016). An adequate required rate of return for grid-connected PV systems. *Solar Energy, 132*, 73–83.
9. Iaquaniello, G., Montanari, W., & Salladini, A. (2017). Standalone CSP-DG system for electrification of remote areas and desalinated water supply. *Solar Energy, 157*, 1056–1063.
10. Muhsen, D. H., Khatib, T., & Abdulabbas, T. E. (2018). Sizing of a standalone photovoltaic water pumping system using hybrid multi-criteria decision making methods. *Solar Energy, 159*, 1003–1015.
11. Allouhi, A., Saadani, R., Kousksou, T., Saidur, R., Jamil, A., & Rahmoune, M. (2016). Grid-connected PV systems installed on institutional buildings: Technology comparison, energy analysis and economic performance. *Energy and Buildings, 130*, 188–201.
12. Chaibi, Y., Malvoni, M., Chouder, A., Boussetta, M., & Salhi, M. (2019). Simple and efficient approach to detect and diagnose electrical faults and partial shading in photovoltaic systems. *Energy Conversion and Management, 196*, 330–343.
13. Gao, X., Li, S., & Gong, R. (2013). Maximum power point tracking control strategies with variable weather parameters for photovoltaic generation systems. *Solar Energy, 93*, 357–367.
14. Ikegami, T., Maezono, T., Nakanishi, F., Yamagata, Y., & Ebihara, K. (2001). Estimation of equivalent circuit parameters of PV module and its application to optimal operation of PV system. *Solar Energy Materials and Solar Cells, 67*, 389–395.
15. Dileep, G., & Singh, S. N. (2017). Application of soft computing techniques for maximum power point tracking of SPV system. *Solar Energy, 141*, 182–202.
16. Gupta, A., Chauhan, Y. K., & Pachauri, R. K. (2016). A comparative investigation of maximum power point tracking methods for solar PV system. *Solar Energy, 136*, 236–253.

17. Hahm, J., Baek, J., Kang, H., Lee, H., & Park, M. (2015). Matlab-based modeling and simulations to study the performance of different MPPT techniques used for photovoltaic systems under partially shaded conditions. *International Journal of Photoenergy, 2015*, 1–11.
18. Salman, S., Ai, X., & Wu, Z. (2018). Design of a P-&-O algorithm based MPPT charge controller for a stand-alone 200W PV system. *Protection and Control Modern Power Systems*, *3*, 25.
19. Alik, R., & Jusoh, A. (2017). Modified perturb and observe (P&O) with checking algorithm under various solar irradiation. *Solar Energy, 148*, 128–139.
20. Alik, R., & Jusoh, A. (2018). An enhanced P&O checking algorithm MPPT for high tracking efficiency of partially shaded PV module. *Solar Energy, 163*, 570–580.
21. Kollimalla, S. K., Member, S., Mishra, M. K., & Member, S. (2014). Variable perturbation size adaptive P & O MPPT algorithm for sudden changes in irradiance. *IEEE Transactions on Sustainable Energy, 5*, 718–728.
22. Hong, Y., Pham, S. N., Yoo, T., Chae, K., Baek, K. H., & Kim, Y. S. (2015). Efficient maximum power point tracking for a distributed PV system under rapidly changing environmental conditions. *IEEE Transactions on Power Electronics, 30*, 4209–4218.
23. Tey, K. S., & Mekhilef, S. (2014). Modified incremental conductance MPPT algorithm to mitigate inaccurate responses under fast-changing solar irradiation level. *Solar Energy, 101*, 333–342.
24. Motahhir, S., Ghzizal, A. E., Sebti, S., & Derouich, A. (2018). Modeling of Photovoltaic System with modified Incremental Conductance Algorithm for fast changes of irradiance. *International Journal of Photoenergy, 2018*, 13.
25. Motahhir, S., El Ghzizal, A., Sebti, S., & Derouich, A. (2017). MIL and SIL and PIL tests for MPPT algorithm. *Cogent Engineering, 4*, 1–18.
26. Loukriz, A., Haddadi, M., & Messalti, S. (2016). Simulation and experimental design of a new advanced variable step size incremental conductance MPPT algorithm for PV systems. *ISA Transactions, 62*, 30–38.
27. Liu, F., Duan, S., Liu, F., Liu, B., & Kang, Y. (2008). A variable step size INC MPPT method for PV systems. *IEEE Transactions on Industrial Electronics, 55*, 2622–2628.
28. Ahmed, E. M., & Shoyama, M. (2011). Stability study of variable step size incremental conductance/impedance MPPT for PV systems. In *8th Int Conf Power Electron - ECCE Asia Green World with Power Electron ICPE 2011-ECCE Asia* (pp. 386–392).
29. Chen, Y. T., Jhang, Y. C., & Liang, R. H. (2016). A fuzzy-logic based auto-scaling variable step-size MPPT method for PV systems. *Solar Energy, 126*, 53–63.
30. Dabra, V., Paliwal, K. K., Sharma, P., & Kumar, N. (2017). Optimization of photovoltaic power system: A comparative study. *Protection and Control of Modern Power Systems, 2*, 3.
31. Kulaksiz, A. A., & Akkaya, R. (2012). A genetic algorithm optimized ANN-based MPPT algorithm for a stand-alone PV system with induction motor drive. *Solar Energy, 86*, 2366–2375.
32. Ramos-Hernanz, J. A., Barambones, O., Lopez-Guede, J. M., Zamora, I., Eguia, P., & Farhat, M. (2016). Sliding mode real-time control of photovoltaic systems using neural estimators. *International Journal of Photoenergy, 2016*, 16.
33. Salas, V., Olías, E., Barrado, A., & Lázaro, A. (2006). Review of the maximum power point tracking algorithms for stand-alone photovoltaic systems. *Solar Energy Materials & Solar Cells, 90*, 1555–1578.
34. Bianconi, E., Calvente, J., Giral, R., Mamarelis, E., Petrone, G., Ramos-Paja, C. A., et al. (2013). A fast current-based MPPT technique employing sliding mode control. *IEEE Transactions on Industrial Electronics, 60*, 1168–1178.
35. Mamarelis, E., Petrone, G., & Spagnuolo, G. (2014). Design of a sliding-mode-controlled SEPIC for PV MPPT applications. *IEEE Transactions on Industrial Electronics, 61*, 3387–3398.
36. Kim, I.-S. (2007). Sliding mode controller for the single-phase grid-connected photovoltaic system Il-song. *Solar Energy, 81*, 405–414.
37. Dahech, K., Allouche, M., Damak, T., & Tadeo, F. (2017). Backstepping sliding mode control for maximum power point tracking of a photovoltaic system. *Electric Power Systems Research, 143*, 182–188.
38. Koofigar, H. R. (2016). Adaptive robust maximum power point tracking control for perturbed photovoltaic systems with output voltage estimation. *ISA Transactions, 60*, 285–293.
39. Chaibi, Y., Salhi, M., El-jouni, A., & Essadki, A. (2018). A new method to determine the Parameters of a photovoltaic Panel equivalent circuit. *Solar Energy, 163*, 376–386.
40. Humada, A. M., Hojabri, M., Mekhilef, S., & Hamada, H. M. (2016). Solar cell parameters extraction based on single and double-diode models: A review. *Renewable and Sustainable Energy Reviews, 56*, 494–509.
41. Chtita, S., Chaibi, Y., Derouich, A., & Belkadid, J. (2019). Modeling and Simulation of a Photovoltaic Panel Based on a Triple Junction Cells for a Nanosatellite. In *Int Symp Adv Electr Commun Technol ISAECT 2018 - Proc* (pp. 1–6).
42. Kchaou, A., Naamane, A., Koubaa, Y., & M'sirdi, N. (2017). Second order sliding mode-based MPPT control for photovoltaic applications. *Solar Energy, 155*, 758–769.
43. Barth, N., Jovanovic, R., Ahzi, S., & Khaleel, M. A. (2016). PV panel single and double diode models: Optimization of the parameters and temperature dependence. *Solar Energy Materials & Solar Cells, 148*, 87–98.
44. Chaibi, Y., & Salhi, M. (2019). Sliding mode controllers for standalone PV systems: Modeling and approach of control. *International Journal of Photoenergy, 2019*, 12.
45. Duffie, J. A., Beckman, W. A., & Worek, W. M. (2003). *Solar Engineering of Thermal Processes, 4nd ed. vol. 116.*
46. Gilman, P. (2015). SAM photovoltaic model technical reference SAM photovoltaic model technical reference. *Solar Energy, 63*, 323–333.
47. Blair, N., Dobos, A. P., Freeman, J., Neises, T., Wagner, M., Ferguson, T., et al. (2014). *System advisor model, sam 2014.1. 14: General description. NREL Rep No TP-6A20–61019* (Vol. 13). CO: Natl Renew Energy Lab Golden.